Electrical Tuning of Nonlinearities in Exciton-Polariton Condensates

S. I. Tsintzos,[1,*] A. Tzimis,[1,2] G. Stavrinidis,[1] A. Trifonov,[3] Z. Hatzopoulos,[1,4] J. J. Baumberg,[5] H. Ohadi,[5,6] and P. G. Savvidis[1,2,3,†]

[1]*Foundation for Research and Technology-Hellas, Institute of Electronic Structure and Laser, P.O. Box 1527, 71110 Heraklion, Crete, Greece*

[2]*Department of Materials Science and Technology, University of Crete, P.O. Box 2208, 71003 Heraklion, Crete, Greece*

[3]*Spin Optics Laboratory, Saint Petersburg State University, Saint Petersburg 198504, Russia*

[4]*Department of Physics, University of Crete, 71003 Heraklion, Crete, Greece*

[5]*NanoPhotonics Centre, Cavendish Laboratory, University of Cambridge, Cambridge CB3 0HE, United Kingdom*

[6]*SUPA, School of Physics and Astronomy, University of St Andrews, St Andrews KY16 9SS, United Kingdom*

(Received 26 January 2018; revised manuscript received 26 April 2018; published 16 July 2018)

A primary limitation of the intensively researched polaritonic systems compared to their atomic counterparts for the study of strongly correlated phenomena and many-body physics is their relatively weak two-particle interactions compared to disorder. Here, we show how new opportunities to enhance such on-site interactions and nonlinearities arise by tuning the exciton-polariton dipole moment in electrically biased semiconductor microcavities incorporating wide quantum wells. The applied field results in a twofold enhancement of exciton-exciton interactions as well as more efficiently driving relaxation towards low energy polariton states, thus, reducing condensation threshold.

DOI: 10.1103/PhysRevLett.121.037401

Achieving the nonlinear quantum regime in photonics where the single-site effective photon interaction energy is larger than the losses opens a plethora of interesting phenomena such as photon blockade [1], photon crystallization [2], and opportunities to realize quantum simulators for the study of condensed matter problems such as Mott-insulator to superfluid phase transitions [3] in arrays of optical cavities. So far, the lack of scalable devices with sufficient nonlinearities and low-enough losses has been the main obstacle for the experimental realization of these phenomena. Exciton polaritons are composite quasiparticles resulting from the strong coupling of cavity photons and quantum well (QW) excitons embedded within a microcavity (MC) [4]. Polaritons interact nonlinearly due to their excitonic component and can form macroscopically coherent condensates [5]. They are scalable to form arrays by either etching [6–8] or optical patterning [9–11] of the microcavity. However, in the presently studied systems, polariton-polariton interaction energy is smaller as compared to their line broadening. There are two approaches towards overcoming this problem: manufacturing higher quality microcavities or enhancing the polariton nonlinearities.

Here, we take the second approach and demonstrate twofold enhancement of the polariton-polariton interaction using wide QWs in an electrically driven MC. By exploiting the quantum confined Stark effect (QCSE) to form dipolar polaritons, we demonstrate tuning of the exciton-exciton interaction. As a direct consequence of this, we obtain an enhancement of the polariton emission in both linear and lasing regimes with a simultaneous reduction of the polariton lasing threshold and shorter polariton condensate formation times due to enhanced exciton scattering. Our results are the first demonstration of the electrical tuning of nonlinearities in exciton-polariton condensates.

Exciton-exciton interactions play a key role in the strong nonlinearities present in MC polariton systems. A first attempt to control these interactions previously suggested, was to utilize the concept of dipolaritons [12] by incorporating double asymmetric quantum wells in an electrically biased MC. Both direct (DX) and indirect (IX) excitons couple to the same cavity mode, forming a new type of polariton with similar properties to the exciton-polariton system. Under this scheme, the coupled DX and IX share the strong oscillator strength of the direct component and the strong dipole moment of the indirect one, favoring higher polariton-polariton interactions. More recently [13], by integrating wide QWs in a simple waveguide, the formation of dipolar polaritons was observed resulting in higher interactions and, therefore, increased energy blueshifts when electric bias was applied. However, in both implementations, only low density linear regimes are considered without examining the consequences of such enhancements on nonlinearities and the polariton condensation regime.

In Fig. 1(a), the schematic of the electrically contacted MC device is illustrated. Four sets of three 18 nm/7 nm $GaAs/Al_{0.3}Ga_{0.7}As$ QWs are embedded, at the maximum of the stationary cavity field, between the top (bottom) undoped $AlAs/Al_{0.15}Ga_{0.85}As$ 25 (29) distributed Bragg reflectors (DBRs). An initial etch down to the last few DBR

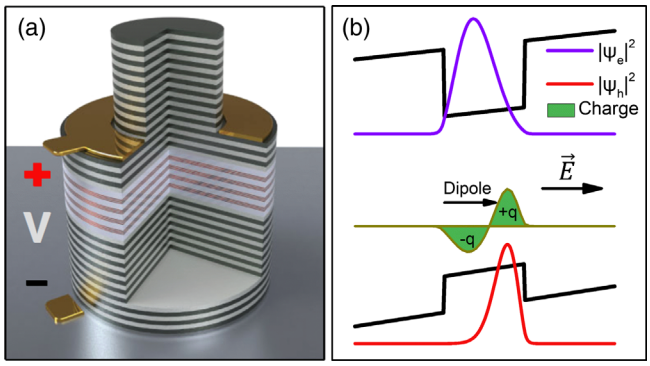

FIG. 1. (a) Schematic illustration of the electrically gated wide QW MC. (b) Schematic representation of electron and hole wave functions in a wide QW under the presence of electric field and the corresponding charge distribution.

layers forms an annular recess onto which the top contact is deposited. A second vertical etch follows for the mesa formation providing electrical isolation of the devices, while evaporation of the back contact onto the $n+$ substrate completes the processing procedure. The uniformity of the applied electric field across the active region is ensured by the high out-of-plane resistivity at the interfaces formed by alternating DBR layers.

In inorganic semiconductor MC systems, the dominating scattering mechanism contributing to the intensity of the lower polariton branch (LPB) luminescence and formation of polariton condensates via efficient relaxation towards low energy states at the bottom of the LP dispersion curve is exciton-polariton scattering [14,15]. Therefore, the ability to achieve strong nonlinearities required for the single polariton quantum regime as well as improvements in the overall device performance crucially depends on controlling the exciton-polariton interaction strength in such systems.

A unique opportunity to enhance such dipole exciton-polariton interactions is provided through application of an electric field across the MC device. The applied field pushes electrons and holes inside the QW in opposite directions and induces an exciton dipole moment oriented along the growth axes as shown in Fig. 1(b). We quantify the effect of bias on the MC by solving the Schrödinger equation in combination with a variational method for the excitons [16,17] to extract the heavy hole (HH) and light hole exciton oscillator strengths and, thus, radiative times [Fig. 2(a)], dipole moment [Fig. 2(a)], and the excitonic Bohr radius and exciton interaction strength constant g_x [18] [Fig. 2(b)] as a function of the electric field. Increase in exciton radiative time with electric field arises from the decrease in electron and hole wave function overlap due to the QCSE [Fig. 2(a)]. Simultaneously, application of electric field provides control over the exciton-exciton interaction g_x, which arises from (i) exchange interactions (g_{exc}) and (ii) dipole-dipole interactions (g_{dip}). Both contributions are shown in Fig. 2(b) as a function of electric

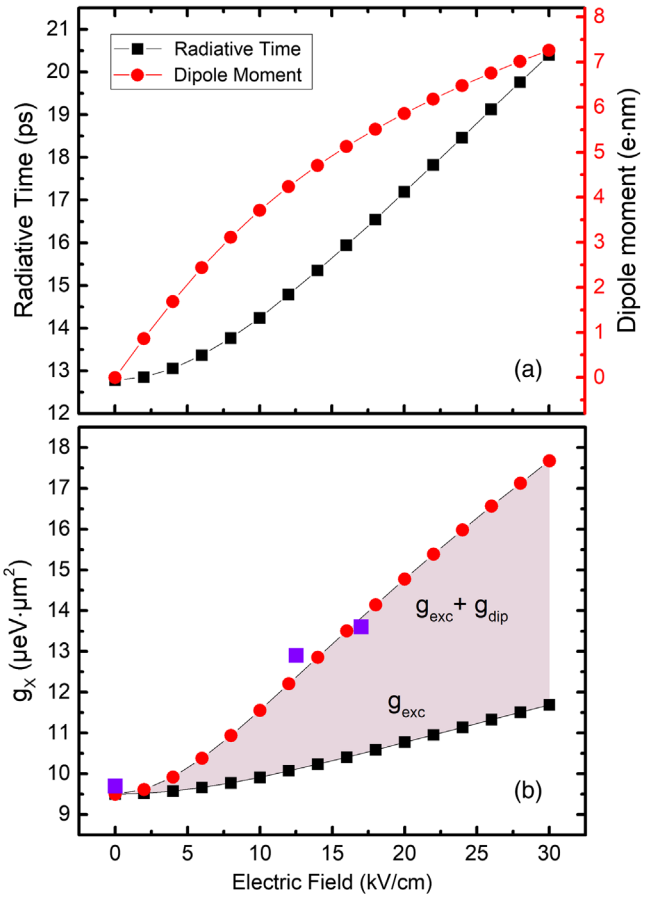

FIG. 2. Theoretical calculations as a function of the electric field for (a) the radiative lifetime and dipole moment for the HH excitons, (b) HH exciton interaction strength. The three purple square points are experimental data exported as discussed in the text.

field. The former depends on the exciton Bohr radius [19] while the latter is enhanced with the increase of the effective dipole length shown in [13].

We initially employ streak camera measurements at 20 K to track the relaxation dynamics in both linear and nonlinear regimes. Notably, since time-resolved photoluminescence (TRPL) experiments directly measure relaxation and scattering dynamics, exciton-polariton interaction strengths which control these processes can be experimentally assessed during the application of electrical bias. In Fig. 3(a), TRPL is recorded for varying electrical bias in the linear low-density excitation regime. For all traces in addition to photoluminescence (PL), we allow a small fraction of pump laser to be collected marking the arrival of the excitation pulse at $t = 0$ ps. Following nonresonant excitation, the PL reaches a maximum at 160 ps and decays over hundreds of ps. We attribute the increase in the integrated PL intensity to enhanced scattering and relaxation of polaritons on the LPB caused by the applied electrical bias. The PL intensity reaches maximum at an applied field of 17 kV/cm, above which LO phonon

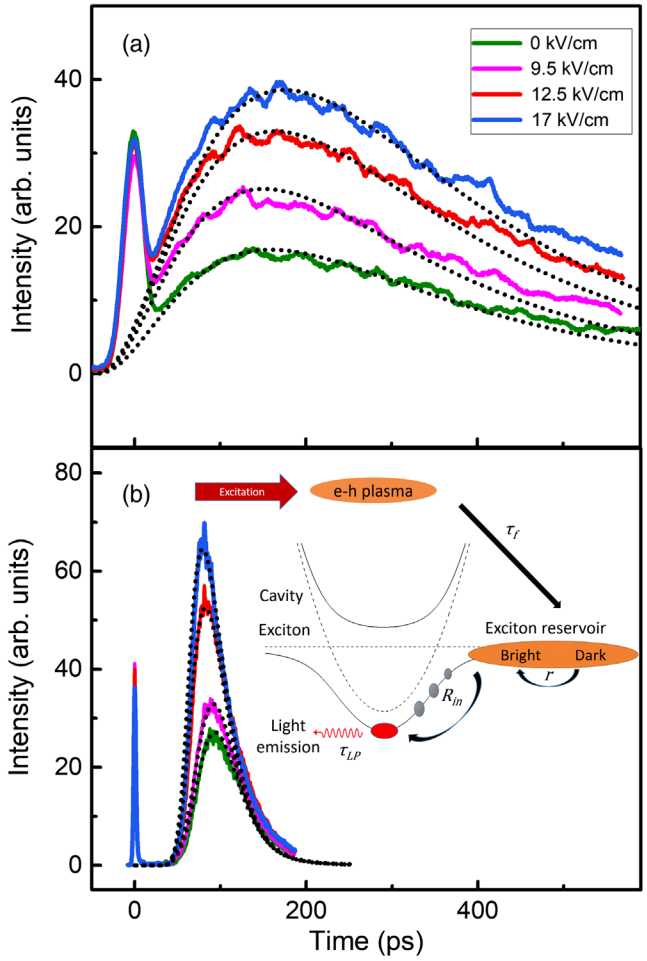

FIG. 3. Time-resolved PL at four discrete electric field values for (a) below laser threshold ($P = 0.2$ mW) and (b) above laser threshold ($P = 4.25$ mW). The inset of (b) is a schematic illustration of the various relaxation mechanisms incorporated in the rate equations.

assisted tunneling between adjacent QWs leads to significant loss in the PL intensity and strong charging of the QWs [20].

Similarly, strong PL intensity enhancements in the presence of electric field is also achieved at higher excitation powers in the polariton lasing regime. Because of the presence of strong nonlinearities and stimulation effects affecting relaxation, the maximum PL intensity and condensation is shifted to earlier times ~90 ps. The sharp rise in the PL intensity at 50 ps marks the time when the system reaches occupancy of one where polariton condensation then dominates the dynamics.

To interpret our experimental results and link PL intensity enhancements to changes in the scattering rates driven by the exciton-polariton interaction strength in both linear and nonlinear regimes, we developed a simplified rate equations model based on the Boltzmann kinetic equations [15], neglecting the momentum-dependence of the various scattering processes. Following the example of [21], we split the reservoir in two parts, labeled as dark and bright, respectively [inset graph in Fig. 3(b)]. The bright excitonic reservoir describes the excitons, with a density n_{BX} that conserves energy and momentum for scattering into the lower polariton branch. The dark excitons, n_{DX}, which are out of the light cone, cannot scatter directly into the condensate, but simply feed the bright subset of excitons with a rate denoted as r through inelastic scattering. To improve the validity of our model, we take into account exciton formation, the radiative and nonradiative exciton losses while the exciton-polariton scattering is considered to be the main process of polariton relaxation to the bottom of the LPB. The detailed equations are shown below while the exact values of the parameters used to fit the experimental data are given in Table 1 in the Supplemental Material [22]:

$$\frac{dn_{eh}(t)}{dt} = P - \frac{n_{eh}(t)}{\tau_{eh}} - \frac{n_{eh}(t)}{\tau_f} \tag{1}$$

$$\frac{dn_{\mathrm{DX}}(t)}{dt} = \frac{n_{eh}(t)}{\tau_f} - \frac{n_{\mathrm{DX}}(t)}{\tau_{\mathrm{nr}}} - r\left[\frac{n_{\mathrm{DX}}(t)}{k} - n_{\mathrm{BX}}(t)\right] \tag{2}$$

$$\frac{dn_{\mathrm{BX}}(t)}{dt} = r\left[\frac{n_{\mathrm{DX}}(t)}{k} - n_{\mathrm{BX}}(t)\right] - \frac{n_{\mathrm{BX}}(t)}{\tau_{\mathrm{rad}}} - R_{\mathrm{in}} n_{\mathrm{BX}}^2(t)[N_{\mathrm{LP}}(t)+1] + R_{\mathrm{out}} n_{\mathrm{BX}} N_{\mathrm{LP}}(t) \tag{3}$$

$$\frac{N_{\mathrm{LP}}(t)}{dt} = R_{\mathrm{in}} n_{\mathrm{BX}}^2(t)[N_{\mathrm{LP}}(t)+1] - R_{\mathrm{out}} n_{\mathrm{BX}} N_{\mathrm{LP}}(t) - \frac{N_{\mathrm{LP}}(t)}{\tau_{\mathrm{LP}}} \tag{4}$$

Here, k is the equilibration rate of the densities between the two reservoirs, n_{eh} is the density of free carriers, while N_{LP} is the population of the polariton ground state. The time constants τ_{eh} and τ_f refer to the free carrier lifetime and the exciton formation time, τ_{nr} the nonradiative lifetime of the dark excitons, τ_{rad} the radiative lifetime of the bright excitons, $R_{\mathrm{in,out}}$ are the scattering rates into and out of the LPB to the bright exciton reservoir and τ_{LP} is the polariton lifetime. We approximate the inscattering and outscattering rates as $R_{\mathrm{in}} = \gamma \exp(-\varepsilon/kT)$ and $R_{\mathrm{out}} = R_{\mathrm{in}} \exp(-\varepsilon/kT)$ [23], where $\varepsilon = -10$ meV is the energy difference between the HH exciton and the minimum of the LPB at 14 K under zero external field, while γ is a parameter which quantifies the electric field dependence of the inscattering rate. Furthermore, we account for both the exciton redshift and the reduction of oscillator strength changes related to application of the external electric field which affects both Hopfield coefficients and polariton lifetimes τ_{LP} using the three harmonic oscillator model.

Excellent agreement between the measured and the modeled PL intensity traces (dotted lines) can be seen in Figs. 3(a) and 3(b). In the present model, only one fitting parameter changes with electric field, namely γ which

quantifies the field dependent polariton relaxation rate. The observed PL enhancement, in both linear and nonlinear regimes, arises from: (a) the increase in exciton radiative lifetime, with increasing electric field, which suppresses PL emission near the relaxation bottleneck and enhances PL emission near $k_{\|} = 0$, and (b) the increase in the exciton-exciton interaction strength which enhances relaxation towards $k_{\|} = 0$ polariton states. Incorporating previously calculated theoretical values for the exciton radiative lifetime, keeping the remaining parameters constant (including the exciton scattering rate), the model predicts only weak enhancement in the PL intensity resulting from any reduction in bright exciton reservoir radiative losses, which is not sufficient to fit our experimental data. Clearly, at high electric fields the second term related to exciton-polariton scattering dominates and contributes strongly to the PL increase. Taking this into account, experimental data both in the linear and nonlinear regimes at electric fields of 12.5 and 17 kV/cm can be fit using higher γ parameter values of $105\,\mu\mathrm{m}^4\,\mathrm{ps}^{-1}$ and $150\ \mu\mathrm{m}^4\,\mathrm{ps}^{-1}$ compared to zero bias scattering time of $56\ \mu\mathrm{m}^4\,\mathrm{ps}^{-1}$ (see, also, Table 1 in the Supplemental Material [22]). This corresponds to enhancements of the inscattering rate R_{in} by a factor of 87% and 267%, respectively. Since the exciton-polariton scattering rate is proportional to $X_{\mathrm{LP}}g_x^2$, where X_{LP} is the excitonic fraction at the LPB [24], the experimentally obtained scattering rate enhancements can be compared with the corresponding electric field induced changes in the exciton interaction constant g_x. Using theoretical values for g_x shown in Fig. 2(d), the calculated field induced changes in the exciton-polariton scattering rate are estimated as 78% and 258% and are in excellent quantitative agreement with the experiment.

Independent estimates of exciton-exciton interaction strength g_x can be obtained performing cw power dependent measurements of the LPB energy blueshifts while varying electrical bias. Assuming that the LPB blueshift depends on the exciton fraction in the LPB $k_{\|} = 0$ state, we select a device with a smaller exciton-photon detuning (−4.5 meV) which permits more precise measurement of g_x. Two indicative sets of PL data, recorded from the LPB zero k state at 20 K, at the same excitation power for zero and 12.5 kV/cm electric field values are plotted in Fig. 4(a), while the extracted blueshift energy is shown in Fig. 4(b). As expected, the gradual energy blueshift slope changes with the increasing electric field, providing evidence for enhanced dipole-dipole interactions. Using the experimentally obtained dark reservoir carrier lifetimes, we calibrate the horizontal axis to obtain the steady state carrier density N and estimate the exciton-polariton interaction constant g_{xp} by fitting the relation $\Delta E = g_{xp}N$ to the linear part of the data shown in Fig. 4(c). This yields $g_{xp} = 2.35\ \mu\mathrm{eV}\,\mu\mathrm{m}^2$ at $F = 0$ kV/cm, $g_{xp} = 3.98\ \mu\mathrm{eV}\,\mu\mathrm{m}^2$ at $F = 12.5$ kV/cm, and $g_{xp} = 4.7\ \mu\mathrm{eV}\,\mu\mathrm{m}^2$ at $F = 17$ kV/cm.

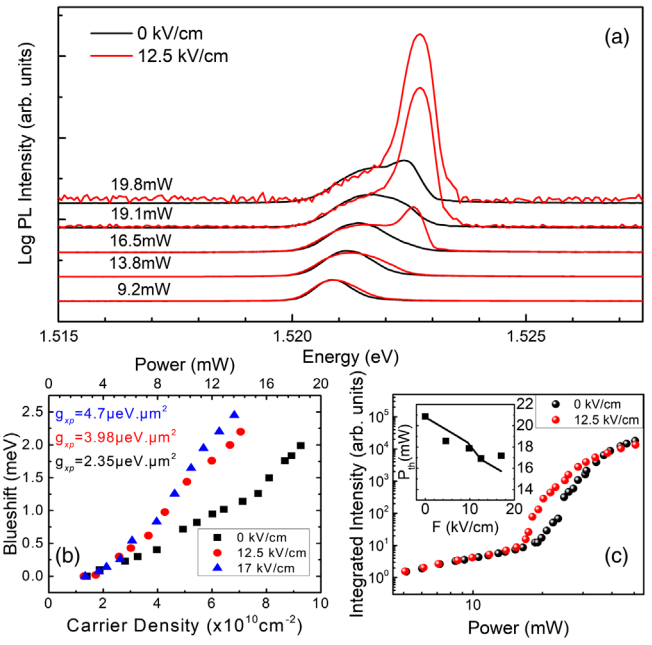

FIG. 4. (a) Logarithmic power dependent PL spectra at zero (black) and 12.5 kV/cm (red) electric fields. (b) The polariton energy blueshift at three different electric field values. (c) Integrated PL emission extracted from the corresponding spectra of (a). Reduction of polariton laser threshold versus electric field appears in the inset. The squares are experimental data while the solid line is obtained from theoretical calculations.

To obtain exciton-exciton interaction strengths from the corresponding exciton-polariton total, the latter has to be normalized by field-dependent exciton Hopfield coefficients [25]. For the electric field values above, after correcting for the exciton fraction, we find $g_x = 9.85\ \mu\mathrm{eV}\,\mu\mathrm{m}^2$ (0 kV/cm), $g_{xp} = 12.98\ \mu\mathrm{eV}\,\mu\mathrm{m}^2$ (12.5 kV/cm), and $g_{xp} = 13.6\ \mu\mathrm{eV}\,\mu\mathrm{m}^2$ (17 kV/cm). These experimental values are in agreement with the theoretical ones presented in the Fig. 2(d). Moreover, direct calculation of the exciton-polariton scattering rate using the above extracted g_x values reveals an enhancement of 83% (12.5 kV/cm) and 250% (17 kV/cm), respectively, which are in agreement with the values found through the rate equation model.

The integrated PL emission extracted from the spectra in Fig. 4(a), is shown in Fig. 4(c). The field-dependent exciton-polariton scattering rate gradually lowers the polariton lasing threshold as shown in the inset of Fig. 4(a) where experimental measurements are shown by squares while the solid line is obtained from the steady state solution of the rate equations by fixing the polariton occupation number $N_{\mathrm{LP}} = 1$. Polariton lasing threshold reduction up to 20% is achieved at the maximum applied electric field of 17 kV/cm.

In conclusion, we demonstrate electrical manipulation of the exciton-exciton interaction strength by applying an external electric field to a wide-QW microcavity. Equivalent results are obtained for the exciton-exciton

interaction constant using time-resolved PL and cw power dependent blueshift measurements. We construct a theoretical model which is in good agreement with and interprets our experimental findings. All of the above corroborate the possibility of manipulating polariton-polariton interactions through external electrical fields. Furthermore, with careful band-structure design and device optimization, allowing application of stronger electric fields, it will be possible to obtain even higher nonlinearities. Such controlled enhancement of exciton interactions, may prove crucial for realization of non-classical light sources relying on the polariton quantum blockade [26].

S. T. acknowledges the financial support of the Stavros Niarchos Foundation within the framework of the project ARCHERS, P. S. acknowledges support form the bilateral Greece-Russia Polisimulator project cofinanced by Greece and the EU Regional Development Fund, A. T. acknowledges the Russian-Greek support from the project supported by the Ministry of Education and Science of The Russian Federation (Project No. RFMEFI61617X0085).

*simostsi@physics.uoc.gr
†psav@materials.uoc.gr

[1] K. M. Birnbaum, A. Boca, R. Miller, A. D. Boozer, T. E. Northup, and H. J. Kimble, Nature (London) **436**, 87 (2005).
[2] D. E. Chang, V. Gritsev, G. Morigi, V. Vuletic, M. D. Lukin, and E. A. Demler, Nat. Phys. **4**, 884 (2008).
[3] M. Greiner, O. Mandel, T. Esslinger, T. W. Hnsch, and I. Bloch, Nature (London) **415**, 39 (2002).
[4] C. Weisbuch, M. Nishioka, A. Ishikawa, and Y. Arakawa, Phys. Rev. Lett. **69**, 3314 (1992).
[5] J. Kasprzak, M. Richard, S. Kundermann, A. Baas, P.Jeambrun, J. M. Keeling, F. M. Marchetti, M. H. Szymanska, R. Andre, J. L. Staehli, V. Savona, P. B. Littlewood, B. Deveaud, and Le S. Dang, Nature (London) **443**, 409 (2006).
[6] E. Wertz, L. Ferrier, D. D. Solnyshkov, R. Johne, D. Sanvitto, A. Lematre, I. Sagnes, R. Grousson, A. V. Kavokin, P. Senellart, G. Malpuech, and J. Bloch, Nat. Phys. **6**, 860 (2010).
[7] T. Gao, P. S. Eldridge, T. C. H. Liew, S. I. Tsintzos, G. Stavrinidis, G. Deligeorgis, Z. Hatzopoulos, and P. G. Savvidis, Phys. Rev. B **85**, 235102 (2012).
[8] L. Ferrier, E. Wertz, R. Johne, D. D. Solnyshkov, P. Senellart, I. Sagnes, A. Lemaitre, G. Malpuech, and J. Bloch, Phys. Rev. Lett. **106**, 126401 (2011).
[9] G. Tosi, G. Christmann, N. G. Berloff, P. Tsotsis, T. Gao, Z. Hatzopoulos, P. G. Savvidis, and J. J. Baumberg, Nat. Phys. **8**, 190 (2012).
[10] A. Askitopoulos, K. Kalinin, T. C. H. Liew, P. Cilibrizzi, Z. Hatzopoulos, P. G. Savvidis, N. G. Berloff, and P. G. Lagoudakis, Phys. Rev. B **93**, 205307 (2016).
[11] H. Ohadi, A. J. Ramsay, H. Sigurdssom, Y. del Valle-Inclan Redondo, S. I. Tsintzos, Z. Hatzopoulos, T. C. H. Liew, I. A Shelykh, Y. G. Rubo, P. G. Savvidis, and J. J. Baumberg, Phys. Rev. Lett. **119**, 067401 (2017).
[12] P. Cristofolini, G. Christmann, S. I. Tsintzos, G. Deligeorgis, G. Konstantinidis, Z. Hatzopoulos, P. G. Savvidis, and J. J. Baumberg, Science **336**, 704 (2012).
[13] I. Rosenberg, Y. Mazuz-Harpaz, R. Rapaport, K. West, and L. Pfeiffer, Phys. Rev. B **93**, 195151 (2016).
[14] G. Malpuech, A. Kavokin, A. Di Carlo, and J. J. Baumberg, Phys. Rev. B **65**, 153310 (2002).
[15] D. Porras, C. Ciuti, J. J. Baumberg, and C. Tejedor, Phys. Rev. B **66**, 085304 (2002).
[16] P. Harrison, *Quantum Wells Wires and Dots: Theoretical and Computational Physics of Semiconductor Nanostructures* (Wiley, Hoboken, NJ, 2005).
[17] E. S. Khramtsov, P. A. Belov, P. S. Grigoryev, I. V. Ignatiev, S. Yu. Verbin, Yu. P. Efimov, S. A. Eliseev, V. A. Lovtcius, V. V. Petrov, and S. L. Yakovlev, J. Appl. Phys. **119**, 184301 (2016).
[18] C. Ciuti, V. Savona, C. Piermarocchi, A. Quattropani, and P. Schwendimann, Phys. Rev. B **58**, 7926 (1998).
[19] T. Byrnes, G. V. Kolmakov, R. Ya. Kezerashvili, and Y. Yamamoto, Phys. Rev. B **90**, 125314 (2014).
[20] P. Tsotsis, S. I. Tsintzos, G. Christmann, P. G. Lagoudakis, O. Kyrienko, I. A. Shelykh, J. J. Baumberg, A. V. Kavokin, Z. Hatzopoulos, P. S. Eldridge, and P. G. Savvidis, Phys. Rev. Applied **2**, 014002 (2014).
[21] G. Nardim, K. G. Lagoudakis, M. Wouters, M. Richard, A. Baas, R. Andre, L. S. Dang, B. Pietka, and B. Deveaud-Pledran, Phys. Rev. Lett. **103**, 256402 (2009).
[22] See Supplemental Material at http://link.aps.org/supplemental/10.1103/PhysRevLett.121.037401 for the exact values of the parameters used to fit the experimental data.
[23] M. Wouters and V. Savona, Phys. Rev. B **79**, 165302 (2009).
[24] F. Tassone and Y. Yamamoto, Phys. Rev. B **59**, 10830 (1999).
[25] R. Hahe, C. Brimont, P. Valvin, T. Guillet, F. Li, M. Leroux, J. Zuniga-Perez, X. Lafosse, G. Patriarche, and S. Bouchoule, Phys. Rev. B **92**, 235308 (2015).
[26] A. Kavokin, J. J. Baumberg, G. Malpuech, and F. P. Laussy, *Microcavities* (Oxford University Press, Oxford, 2007).